

Wavelet correlations to reveal multiscale coupling in geophysical systems

Erik Casagrande¹, Brigitte Mueller², Diego Miralles^{3,4}, Dara Entekhabi⁵ and

Annalisa Molini^{1,*}

arXiv:1502.05255v1 [physics.ao-ph] 18 Feb 2015

* Corresponding author: Annalisa Molini, Institute Center for Water and Environment (iWater), Masdar Institute of Science and Technology, PO Box 54224, Abu Dhabi, UAE (amolini@masdar.ac.ae)

¹Institute Center for Water and Environment (iWater), Masdar Institute of Science and Technology, Abu Dhabi, United Arab Emirates.

²Environment Canada, M3H 5T4, Toronto, Ontario, Canada.

³VU University Amsterdam, Earth and Life Sciences, Amsterdam, The Netherlands.

⁴Ghent University, Laboratory of Hydrology and Water Management, Ghent, Belgium.

⁵Ralph M. Parsons Laboratory for Environmental Science and Engineering, Massachusetts Institute of Technology, Cambridge, Massachusetts, USA.

Abstract. The interactions between climate and the environment are highly complex. Due to this complexity, process-based models are often preferred to estimate the net magnitude and directionality of interactions in the Earth System. However, these models are based on simplifications of our understanding of nature, thus are unavoidably imperfect. Conversely, observation-based data of climatic and environmental variables are becoming increasingly accessible over large scales due to the progress of space-borne sensing technologies and data-assimilation techniques. Albeit uncertain, these data enable the possibility to start unraveling complex multivariable, multiscale relationships if the appropriate statistical methods are applied.

Here, we investigate the potential of the wavelet cross-correlation method as a tool for identifying multiscale interactions, feedback and regime shifts in geophysical systems. The ability of wavelet cross-correlation to resolve the fast and slow components of coupled systems is tested on synthetic data of known directionality, and then applied to observations to study one of the most critical interactions between land and atmosphere: the coupling between soil moisture and near-ground air temperature. Results show that our method is not only able to capture the dynamics of the soil moisture-temperature coupling over a wide range of temporal scales (from days to several months) and climatic regimes (from wet to dry), but also to consistently identify the magnitude and directionality of the coupling. Consequently, wavelet cross-correlations are presented as a promising tool for the study of multiscale in-

teractions, with the potential of being extended to the analysis of causal relationships in the Earth system.

1. Introduction

Natural systems are often characterized by complex interactions, mainly originating in the overlap of dynamical processes acting at very diverse temporal and spatial scales. Examples of this multiscale dynamics can be found in several branches of geophysics. These include climate and the hydrological cycle, whose different components interact and synchronize over a wide range of scales and patterns [Lovejoy and Schertzer, 2013; Tsonis and Elsner, 2007], and ecological systems, where resilience and evolution are mainly determined by cooperation and connectivity [Solé *et al.*, 1998; Moilanen and Nieminen, 2002; Cowen *et al.*, 2006]. In a similar framework it is logical to expect that also the couplings among the different components of the system – and between the system and the surrounding – take place at multiple scales and across them. Multiscale interactions have recently received extensive attention in the literature, and have been proposed as a mechanism for the triggering of extreme events [Miralles *et al.*, 2014; Peters, Debra P. C. *et al.*, 2004; Raffa *et al.*, 2008], abrupt regime transitions [Okin *et al.*, 2009; Peters *et al.*, 2007] and patterns formation [Scanlon *et al.*, 2007; Guttal and Jayaprakash, 2009].

Examples of this increasing interest for multiscale and cross-scale interactions can be found in ecology [Allen and Holling, 2013; Moritz *et al.*, 2005; Cash *et al.*, 2006; Peters *et al.*, 2007; Raffa *et al.*, 2008; Scanlon *et al.*, 2007; Thrush *et al.*, 2013; Werner *et al.*, 2014] and climate dynamics [Holbrook *et al.*, 2014; Debra P. C. Peters *et al.*, 2007; Molini *et al.*, 2010a; Okin *et al.*, 2009; Rial *et al.*, 2004], but also in fields other than geosciences such as network morphology [Ódor, 2013; Pastor-Satorras and Vespignani, 2001] and econometrics [Nikkinen *et al.*, 2011]. Most of these studies are based on minimalist models of

interaction across scales [Allen and Holling, 2002; Peters, Debra P. C. et al., 2004; Peters et al., 2007], or – when some kind of data-driven approach is attempted – on classical scaling statistics, more able to resolve the scale-dependent structure of the considered processes, rather than coupling strength and directionality across scales.

Following this approach, the scaling properties of a wide number of dynamical processes including turbulent flows [Frisch and Kolmogorov, 1995], atmospheric tracers such as precipitation [Molini et al., 2010b; Veneziano and Lepore, 2012; Lovejoy and Schertzer, 2013], ecosystems patterns and organization [Wu, 2006; Nagelkerken, 2009], social networks [Szell et al., 2010], urban growth and development [Lämmer et al., 2006; Chen and Zhou, 2008; Bettencourt et al., 2007; Pumain, 2004], and economic systems [Lux and Marchesi, 1999; Mandelbrot and Stewart, 1998; Mandelbrot, 1997] have been intensively investigated in the last decades through a variety of scaling metrics. In contrast, considerably less attention has been devoted to the analysis of couplings and feedbacks taking place at different scales and across them [Dhamala et al., 2008a; Molini et al., 2010a; Schmitt and Chainais, 2007], to the development of ad-hoc statistics to analyze the temporal evolution of such couplings [Li and Nozaki, 1997; Ngae et al., 1998; Mizuno-Matsumoto et al., 2001; Sello and Bellazzini, 2000; Salvetti et al., 1999; Onorato et al., 1997; Lungarella et al., 2007; Shirazi et al., 2013], and to the investigation of the spectral features of systems displaying strong connectivity across inter-annual, seasonal and sub-seasonal scales [Torrence and Compo, 1998; Torrence and Webster, 1999].

In this study we explore the potential of a simple *local-coupling* metric, the wavelet cross-correlation, for identifying and assessing linear and intermittent interactions across different temporal scales in geophysical systems. Time-domain correlations are routinely

applied to multivariate geophysical time-series to identify phase consistency among the variables, but they fail when the variability is dominated by periodicity or when the phase consistency is intermittent. Harmonics-based statistics equivalent to the time-domain correlation, like spectral coherence and cross-spectra can partially fill this gap, being able to separate the phase consistency over different persistent frequencies. However, also these spectral statistics are limited in capturing interactions that may be transient in time or may display different directionality across scales.

Conversely, wavelet cross-correlation can be inferred through the wavelet decomposition of observed signals, and widens the classical concept of multiscale information flow within random multiplicative processes [Arneodo *et al.*, 1998]. What is particularly appealing in this measure is its ability to decompose linear correlations in scale and time, preserving simultaneously the total correlation of the system [Daubechies, 1992]. Based on the whitening properties of wavelet filters [Mallat, 2008; Percival, 1999], the wavelet coefficients describing the bi-variate process $\{X_t, Y_t\}$ at each temporal scale s can be treated as realizations of the jointly Gaussian random process $\{\mathcal{W}_X(t, s), \mathcal{W}_Y(t, s)\}$ and the sample pairs $(w_X(t_i, s), w_Y(t_i, s))$ and $(w_X(t_j, s), w_Y(t_j, s))$ can be considered mutually independent for $i \neq j$. However, if the joint-Gaussianity assumption can in practice be relaxed when we test null cross-correlations, the *null auto-correlation* hypothesis suffers from a number of limitations – mostly depending on the degree of wavelet overlapping at the analyzed scale – which need to be considered.

The essential theoretical background on wavelet cross-correlation and its significance testing are discussed in section 2, together with some caveats about the inference of directional couplings from spectral statistics. Section 3 is devoted to test the performance

of the wavelet cross-correlation in assessing scale-by-scale interaction in synthetic autoregressive systems of known directional coupling and increasing complexity. Following the test on synthetic data, section 4 deals with the multiscale nature of land-atmosphere interactions through the example of the air temperature-soil moisture coupling and feedback [Seneviratne *et al.*, 2010, 2006; Miralles *et al.*, 2012; Orlowsky and Seneviratne, 2010]. Finally, a further discussion of wavelet cross-correlation strength and criticality is provided in section 5, together with concluding remarks and future developments.

2. Methods and Background

Wavelet cross-correlations are obtained through the combined use of wavelet filtering [Mallat, 2008; Daubechies, 1992] and classic linear coupling measures.

In the time domain, under stationary and ergodic assumptions, the simplest and most adopted measure of linear coupling between the trajectories of a bi-variate real-valued stochastic process $\{X_t, Y_t\}$ is the cross-correlation function $\rho_{XY}(\tau)$ defined as:

$$\rho_{XY}(\tau) = \frac{\gamma_{XY}(\tau)}{\sqrt{\sigma_X^2 \sigma_Y^2}}, \quad (1)$$

with $\tau = 0, \dots, k$ representing the time lag (i.e. temporal asymmetry) between the process trajectories, $\gamma_{XY}(\tau) = E[X_t Y_{t+\tau}]$ their non-centered covariance, and σ_X^2, σ_Y^2 the variances of $\{X_t|\cdot\}$ and $\{\cdot|Y_t\}$ respectively. Assuming that causes precede effects in time, it is common practice to associate the presence of significant correlations at non-zero lags with causal asymmetric coupling. However, when the analyzed signals display multi-scaling, non-stationarity and periodicity – or simply some form of oscillatory behavior at different frequencies – causality can hardly be inferred from classic lagged cross-correlations [see Granger, 1969, for a detailed discussion of the relationship between causality, co-

integration and correlation]. In fact, it is important to note that even if the analyzed signals are expected to display different coupling strengths and synchronization patterns over a wide range of temporal scales – like often the case in climate and other geophysical systems – what we finally “see” through the estimation of $\rho_{XY}(t, t + \tau)$ is only the aggregated effect of these multiscale interactions, that does not necessary reproduce the actual directionality of the coupling at a specific scale s .

As an example, interactions between land and atmosphere such as the soil moisture-air temperature coupling discussed in section 4, are characterized by strong seasonal synchronization effects that can partially mask the directionality of fine-scale interactions. However, high-frequency components – through vertical fluxes of energy and water acting at extremely localized spatio-temporal scales – still play an important role in triggering and sustaining those interactions. Decomposing the correlation into its scale-by-scale components can hence shade some light on the different dynamical processes characterizing the observed coupling. This can be achieved by simply considering the analogue of lagged correlation in the wavelet domain [*Li and Nozaki, 1997; Turbelin et al., 2008*], i.e. *wavelet cross-correlation*. Unlike integral statistics such as wavelet co-spectra and coherence [*Grinsted et al., 2004; Maraun and Kurths, 2004; Torrence and Compo, 1998*], the wavelet cross-correlation is based on the “a priori” decomposition of the bi-variate signals through wavelet band-pass filtering and on a direct inference of scale-by-scale linear correlations from the resulting time series of sample coefficients $w_{X_i}(t, s)$.

Wavelet cross-correlations were first adopted in a number of experimental studies on multiscale interactions in turbulent flows and mixing [*Li and Nozaki, 1997; Ngae et al., 1998; Sello and Bellazzini, 2000; Salvetti et al., 1999; Onorato et al., 1997*], mainly based

on the continuous wavelet transform (CWT). Following this bulk of work, Whitcher and coauthors [Whitcher and Jensen, 2000; Whitcher et al., 2000] proposed an expression for wavelet cross-correlations and their confidence interval based on the maximum overlap discrete wavelet transform (MODWT), a variant without sub-sampling of the orthonormal discrete wavelet transform (DWT) [Foufoula-Georgiou and Kumar, 1994; Percival and Mofjeld, 1997]. The use of MODWT instead of DWT was dictated by the lack of translation invariance in the latter, strongly impacting the final lag-resolution of wavelet cross-correlations. Through the MODWT, it is also possible to reduce the effects of redundancy, partially preserving invariance in the translation [Gençay et al., 2001].

However, the trade-off between lag-resolution and redundancy should be carefully evaluated depending on the specific application. In this study, based on the wide range of temporal scales over which geophysical processes evolve, and on the necessity of retaining as much information as possible about asymmetry in coupling, we opted for using the CWT together with complex analyzing wavelets, known to preserve these properties [Mallat, 2008]. Also redundancy of CWT cannot be really considered a disadvantage here, until we are not concerned with compression and the effects of auto-correlation at large scales. Rather it can often become an advantage since the redundancy of CWT allows for a better visualization of correlation patterns across scales [Crowley, 2007].

2.1. Continuous Wavelet Filtering: Generalities

Let $x(t)$ denote a sample trajectory of the *finite energy* random process $\{X_t\}$. Then via the CWT, we can decompose $x(t)$ into a set of finite basis functions, representing its *variability* at different scales and instants in time [Mallat, 2008; Daubechies, 1992; Torrence and Compo, 1998].

The coefficients $w_X(u, s)$ of the CWT are obtained by decomposing $x(t)$ over dilated and translated wavelet functions $\psi \in \mathbf{L}^2(\mathbb{R})$ of zero average and $\|\psi\| = 1$:

$$w_X(u, s) = \langle x, \psi_{u,s} \rangle = \int_{-\infty}^{+\infty} x(t) \frac{1}{\sqrt{s}} \psi^* \left(\frac{t-u}{s} \right) dt \quad (2)$$

where s is the wavelet scale (inverse of the pseudo-frequency), u is the translation along the time axis, $\psi^*(\cdot)$ indicates the complex conjugate of the wavelet basis function and $\langle \cdot, \cdot \rangle$ is the inner product. Since each trajectory of $\{X_t\}$ is a sample function from a collection of random variables $\{X_{t_1}, \dots, X_{t_n}\}$ the wavelet filtering process is asymptotically equivalent to decomposing $\{X_t\}$ in a finite number of stochastic processes $\{\mathcal{W}_X(u, s)\}$ whose realizations are the $w_X(u, s)$. In addition, it is easy to prove that the wavelet transform is equivalent to a convolution with dilated band-pass filters [Mallat, 2008, p. 79].

Thus, we can rewrite equation (2) as $w_X(u, s) = x \star \bar{\psi}_s(u)$, with $\bar{\psi}_s(u) = 1/\sqrt{s} \psi^*(-t/s)$ and its Fourier transform given by $\hat{\bar{\psi}}_s(\omega) = \sqrt{s} \hat{\psi}^*(s\omega)$. It follows that since ψ is zero-average, $\hat{\psi}(0)$ is also zero and $\hat{\psi}$ becomes the transfer function of a band-pass filter. The CWT extends the benefits of Fourier analysis to observations involving transients and non-stationarities, allowing the estimation of *local* spectral density metrics such as the wavelet scalogram:

$$W_X(t, s) = |w_X(t, s)|^2, \quad (3)$$

and cross-scalogram:

$$W_{XY}(t, s) = w_X^*(t, s) w_Y(t, s), \quad (4)$$

routinely used as a measure of coupling across scales. However, these and other similar metrics such as the wavelet co-spectrum and the wavelet coherence, are not able to provide any information about the temporal asymmetry of couplings at different scales, unlike wavelet cross-correlation metrics.

2.2. Multiscale Interactions and Wavelet Cross-correlations

We can now define the wavelet covariance of the random process $\{X_t, Y_t\}$ at lag τ and scale s , as:

$$\gamma_{XY}(s, \tau) = E[\mathcal{W}_X^*(t, s)\mathcal{W}_Y(t + \tau, s)] \quad (5)$$

This can be alternatively expressed as [Li and Nozaki, 1997]:

$$\gamma_{XY}(s, \tau) = \frac{s}{2\pi} \int_{-\infty}^{+\infty} S_{XY}(\omega) \left| \hat{\psi}(s\omega) \right|^2 e^{i\tau\omega} d\omega, \quad (6)$$

where $S_{XY}(\omega)$ is the co-spectrum of the two signals and

$$\Gamma_{XY}(\omega, s) = S_{XY}(\omega) \left| \hat{\psi}(s\omega) \right|^2 \quad (7)$$

is the *local wavelet co-spectrum function*. Therefore $\gamma_{XY}(s, \tau)$ is the inverse Fourier transform of the local co-spectrum, that integrated across scales gives the classical covariance among the signals $\gamma_{XY}(\tau)$. Although, if the analyzing wavelet ψ is complex also $\gamma_{XY}(s, \tau)$ is a complex function and can be decomposed into a real part $\Re(\gamma_{XY}(s, \tau))$ and an imaginary part $\Im(\gamma_{XY}(s, \tau))$, bearing information about the strength and the phase of the correlations. It is important to note that in this last case the conservation of $\gamma_{XY}(\tau)$ across scales holds only for the real part of the coefficients [Daubechies, 1992], so that the corresponding *wavelet cross-correlation* $\rho_{XY}(s, \tau)$ is most commonly estimated as [Li and Nozaki, 1997]:

$$\rho_{XY}(s, \tau) = \frac{\Re(\gamma_{XY}(s, \tau))}{\sqrt{\Re(\sigma_X^2(s)) \Re(\sigma_Y^2(s))}}, \quad (8)$$

where the $\sigma_i^2(s)$ represent the variance of the i -th variable coefficients at scale s . This form of wavelet cross-correlation ranges between -1 and 1 like its time domain counterpart, and represents a simple local decomposition of the cross-correlation function in time. Since the co-variance of a bi-variate complex-valued random process $\{\mathcal{W}_X(t, s), \mathcal{W}_Y(t, s)\}$ is given

by:

$$\gamma = (\mathcal{W}_X^{\Re} \mathcal{W}_Y^{\Re} + \mathcal{W}_X^{\Im} \mathcal{W}_Y^{\Im}) + i (\mathcal{W}_X^{\Re} \mathcal{W}_Y^{\Im} - \mathcal{W}_X^{\Im} \mathcal{W}_Y^{\Re}), \quad (9)$$

it is easy to show through symmetry considerations that

$$\Re(\gamma_{XY}(s, \tau)) = 2E[\Re(\mathcal{W}_X(t, s)) \Re(\mathcal{W}_Y(t + \tau, s))]. \quad (10)$$

Therefore, if an analytic wavelet is used in the decomposition, the asymmetry in the coupling at different scales mainly derives from *temporal* shifts among the real parts of the coefficients, rather than from a direct wavelet phase estimation. Figure 1 provides a conceptual representation of wavelet correlation patterns corresponding to X driving Y (d), instantaneous coupling (e) and Y driving X (f) and the associated geometry of sample coefficients at generic scale s_0 (a-c). Here the forcing direction is assumed to be homogeneous across scales like in a red-noise dominated process lacking of characteristic forcing scales.

There are a number of alternative formulations for $\rho_{XY}(s, \tau)$, such as the one recently proposed by *Shirazi et al.* [2013], and based on the amplitudes instead of the real part of the coefficients. This neglects the information about temporal asymmetries to focus only on the amplitude of correlations across diverse scales. *Sello and Bellazzini* [2000] also proposed to estimate scale-by-scale couplings in the form of a local wavelet coherence:

$$\zeta_{XY}(s, \tau) = \frac{2\|\gamma_{XY}(\tau, s)\|^2}{\|\sigma_X^2(s)\|^4 + \|\sigma_Y^2(s)\|^4}. \quad (11)$$

This metric however, varies between 0 and 1 due to the absolute operator at the nominator, thus it cannot provide information about the sign of the coupling.

In the following, $\rho_{XY}(s, \tau)$ is estimated based on the expression in equation (8), which is also the one most directly connected with linear couplings in the time domain. The

corresponding estimator of $\rho_{XY}(s, \tau)$ is then given by:

$$r_{XY}(s, \tau) = \frac{\Re(\sum w_X^*(i, s) w_Y'(i + \tau, s))}{\sqrt{\Re(\sum [w_X'(i, s)]^2) \Re(\sum [w_Y'(i, s)]^2)}}, \quad (12)$$

with $w'(i, s) = w(i, s) - \bar{w}_s$ and \bar{w}_s being the long-term average of coefficients at scale s .

2.3. Complex Wavelet Kernels

Different analyzing wavelets can lead to diverse localization effects in frequency and/or in time, that can become crucial for the identification of scale-dependent directional interactions. For this reason, in the following we estimate sample correlations $r_{XY}(s, \tau)$ by using two analytic wavelets with different localization in time and scale, i.e. the Morlet and the Paul wavelets. The Morlet wavelet is defined as:

$$\psi_{\text{morl}}(\eta) = \pi^{-\frac{1}{4}} e^{i\omega_0\eta - \frac{1}{2}\eta^2}, \quad (13)$$

while the Paul wavelet is given by:

$$\psi_{\text{paul}}(\eta) = \frac{2^m i^m m!}{\sqrt{\pi(2m)!}} (1 - i\eta)^{-(m+1)}, \quad (14)$$

where η is the non-dimensional time parameter, ω_0 the central frequency of the Morlet wavelet and m the order parameter of the Paul wavelet.

The Morlet wavelets are more localized (displaying higher resolution) in frequency than in time, while the Paul wavelets display a higher temporal localization [Torrence and Compo, 1998]. This comparison allows us to address the effects of time/scale resolution on the estimation of the wavelet cross correlations. Following the classic work of Torrence and Compo [1998] we use $\omega_0 = 6$ and $m = 4$ to obtain an effective trade-off in the time and frequency resolution of the decomposition. When working with the Morlet wavelet, the choice of a central frequency $\omega_0 = 6$ is further justified by the fact that Morlet is not a proper wavelet, as its integral is not zero. However, for ω_0 larger than

5, the integral becomes small enough to ensure the numerical applicability of the Morlet kernel [Kumar and Foufoula-Georgiou, 1997]. As complex functions, both the Morlet and Paul wavelets are suitable to study oscillatory time series, and have been extensively used in geosciences [Foufoula-Georgiou and Kumar, 1994; Torrence and Compo, 1998]. In addition, both the Morlet and Paul wavelets are symmetric, allowing for a non-distorted estimation of temporal shifts. This is an important property for robust and reliable analysis of directional couplings. At the same time, we have to keep in mind that being non-orthogonal, their CWT can be affected by an overlapping of sub-frequency bands and consequent redundancies in the decomposition of the analyzed signal.

2.4. Significance Test

Similar to their time-domain counterparts, multiscale correlations can be tested for significance based on a scale-dependent approach. In the following, we introduce a simple significance test for wavelet cross-correlations based on the assumption that the coefficients $(w_X(t_i, s), w_Y(t_i, s))$ are sample pairs drawn from the jointly Gaussian random process $\{\mathcal{W}_X(t, s), \mathcal{W}_Y(t, s)\}$, and that $r_{XY}(s, \tau)$ ($r_{s,t}$ hereafter for simplicity) is the corresponding sample statistic for the correlation strength and direction at scale s . Such an assumption originates from the whitening properties of the wavelet transform [Mallat, 2008; Percival, 1999], and provides us with the necessary machinery to test $r_{s,t}$ against the null correlation hypothesis and construct approximate statistical confidence intervals. We show that in case of *null correlation* the joint-normality condition can be relaxed owing to the asymptotic properties of the sample correlation distribution in $\rho_{s,\tau} = 0$ [Johnson et al., 1994].

In general, the probability distribution of the sample correlation $f_R(r_{s,\tau})$ is cumbersome to derive in a closed-form. One of the simplest expressions is due to Fisher [Fisher, 1915] and is given by:

$$f_R(r_{s,\tau}) = \frac{(1 - \rho_{s,\tau}^2)^{\frac{n-1}{2}}}{\pi \Gamma(n-2)} (1 - r_{s,\tau}^2)^{\frac{n-4}{2}} \frac{d^{n-2}}{d(r_{s,\tau} \rho_{s,\tau})^{n-2}} \left\{ \frac{\cos^{-1}(-r_{s,\tau} \rho_{s,\tau})}{\sqrt{(1 - \rho_{s,\tau}^2 r_{s,\tau}^2)}} \right\} \quad (15)$$

where $\Gamma(\cdot)$ is the Gamma function and n the sample size. Equation (15), although written in terms of elementary functions, is still too complex to be explicitly used in testing. However, for $\rho_{s,\tau} = 0$ it reduces to the null pdf proposed in 1908 by Student [Kendall and Stuart, 1945; Johnson et al., 1994]:

$$\begin{aligned} f_R(r_{s,\tau}) &= \frac{1}{B\left(\frac{n-2}{2}, \frac{1}{2}\right)} (1 - r_{s,\tau}^2)^{\frac{n-4}{2}} \\ &= \frac{\Gamma\left(\frac{n-1}{2}\right)}{\Gamma\left(\frac{1}{2}\right) \Gamma\left(\frac{n-2}{2}\right)} (1 - r_{s,\tau}^2)^{\frac{n-4}{2}}, \end{aligned} \quad (16)$$

where $B(\cdot)$ is the Beta function. Contrary to sample distributions for $\rho \neq 0$ – known to be markedly asymmetric – the probability density function in equation (16) is symmetric around 0 and its derived distribution for

$$t_{s,\tau} = \frac{r_{s,\tau}}{\sqrt{(1 - r_{s,\tau}^2)}} \sqrt{(n-2)}, \quad (17)$$

reduces to a t-Student with $(n-2)$ degrees of freedom:

$$f_T(t_{s,\tau}) = \frac{1}{\sqrt{(n-2)} B\left(\frac{n-2}{2}, \frac{1}{2}\right)} \left(1 + \frac{t_{s,\tau}^2}{n-2}\right)^{-\frac{n-1}{2}}. \quad (18)$$

Therefore, once defined a significance level α , equations (17) and (18) can be used to test wavelet cross-correlations $r_{s,\tau}$ against the hypothesis $H_0 : \rho_{s,\tau} = 0$, whose two-tailed rejection region lies outside $[-t_{\alpha/2, n-2}, t_{\alpha/2, n-2}]$. An alternative approach, often adopted

in the literature to test the hypothesis $\rho > \rho'$ for $\rho' \neq 0$, relies on a variance-equalizing transformation known as Fisher z -transformation:

$$Z_{s,\tau} = \tanh^{-1} r_{s,\tau} = \frac{1}{2} \log \left(\frac{1 + r_{s,\tau}}{1 - r_{s,\tau}} \right), \quad (19)$$

where Z is approximately normally distributed with mean $\mu_z = (1/2) \ln[(1+\rho_{s,\tau})/(1-\rho_{s,\tau})]$ and variance $\sigma_z^2 = 1/(n-3)$. However in this study we limit the approach to test the absence of correlation across scales.

This choice is motivated by the superior robustness of the $r_{s,\tau}$ estimator in $\rho = 0$, and to the possibility of widening the usage of null distribution in equation (16) to non jointly-Gaussian samples [Johnson *et al.*, 1994]. In fact, while the expression in equation (16) can be seen as an exact representation of f_R in $\rho = 0$, Fisher's transformation only represents an approximation of f_R away from 0. Consequently, assuming that linearity and homoscedasticity conditions hold, the f_R in $\rho = 0$ always coincides with the null distribution of a jointly-normal process, while the non null distribution of r is robust only under additional kurtosis constrains [see Johnson *et al.*, 1994, p.582]. It is also worth noting that the transformation in equation (18) is generally assumed to be less sensitive to violations of the normality assumption [Edgell and Noon, 1984; Havlicek and Peterson, 1977], i.e. deviations of $\{\mathcal{W}_X(t, s), \mathcal{W}_Y(t, s)\}$ from a jointly Gaussian distribution should not impact the test for null correlation across scales.

In geosciences it is also a common practice to test spectral statistics – such as wavelet co-spectra and coherence – against alternative null hypotheses based on the background noise of the underlying process [Torrence and Webster, 1999]. The statistical significance at the desired significance level α is therefore obtained numerically via Monte Carlo simulations. For example, in the case of a red background noise, the null hypothesis is obtained

by Monte Carlo replicates [Torrence and Webster, 1999] through the following steps: (a) a first order autoregressive model of the background noise is fitted to the observed data; (b) a set of surrogates is generated from the fitted model and (c) a suitable confidence interval is computed producing the desired quantile bounds. However, this numerical approach has been shown to lead to spurious significant correlations in case of reduced samples [Maraun and Kurths, 2004; Maraun et al., 2007]. Also, it implies strong assumptions on the background noise of the observed processes.

3. Wavelet Cross-correlation from Auto-regressive Systems with Pseudo-periodic Features

In this section we test the ability of the wavelet cross-correlation $r_{s,\tau}$ to capture multi-scale interactions in synthetic processes of known directional coupling. Large ensembles of numerically generated time series are used to understand whether $r_{s,\tau}$ can be used as an efficient estimator of scale-by-scale coupling strength and directionality for systems of increasing complexity.

3.1. Coupling in a First-Order Vector Auto-regressive System

The first case study we consider is a simple first order vector auto-regressive model (VAR(1)) in the form:

$$\begin{bmatrix} x(t) \\ y(t) \end{bmatrix} = \begin{bmatrix} 0.80 & C_1 \\ C_2 & 0.70 \end{bmatrix} \begin{bmatrix} x(t-1) \\ y(t-1) \end{bmatrix} + \begin{bmatrix} \epsilon(t) \\ \xi(t) \end{bmatrix}, \quad (20)$$

where C_1 and C_2 are coupling parameters defining the strength and directionality of the interaction between x and y , and $\epsilon(t)$ and $\xi(t)$ are uncorrelated noise terms with zero mean and unitary variance. Figure 2a shows a realization of the VAR(1) model in equation (20), where the x and y sub-spaces were linked in a unidirectional way by imposing a coupling

coefficient $C_1 = -0.4$ ($y \rightarrow x$), and a null feedback from x to y ($C_2 = 0$). Panel b of the same figure reports the corresponding theoretical power spectra for the x (blue dashed line) and y (green solid line) autoregressive sub-spaces, whose Lorentzian decay is typified by the absence of characteristic scales of autocorrelation. VAR(1) models, even though simple in construct, still represent a valuable benchmark for $r_{s,\tau}$. Red noise, or more in general $1/f^\alpha$ noise spectral decay is in fact a characteristic feature of many geophysical systems [Agnew, 1992; Keshner, 1982; Muzzy *et al.*, 2011]. In these models the strength and directionality of the coupling can be easily – and intuitively – tuned. Also, the absence of a characteristic scale for the coupling is reflected in “cascade-like” $r_{s,\tau}$ patterns similar to the ones sketched in Figure 1.

Figure 3a-d shows the $r_{s,\tau}$ computed from both single and ensemble-realizations of the VAR(1) model in equation (20) for different values of the coupling parameters C_1 and C_2 . Each ensemble includes 100 realizations of sample size $n = 4096$, independently generated starting from random initial conditions. The wavelet cross-correlation $r_{s,\tau}$ is estimated as an ensemble average over all the 100 realizations based on a Paul mother wavelet of order $m = 4$, and thus represented as a function of temporal asymmetry τ on the abscissas and scale s on the ordinates. Figure 3a depicts the scale-by-scale correlation patterns resulting from imposing a strong negative coupling from x to y ($C_2 = -0.9$) and null feedback from y to x ($C_1 = 0$), while Figure 3b shows a case with opposite and weaker coupling, i.e. $C_1 = -0.4$ and $C_2 = 0$. The considered VAR(1) systems are therefore both negatively coupled but with different strengths, and feedback effects are not considered at this stage. Correlations below the $\alpha = 99\%$ significance level are masked in white.

It is interesting to note how in a vector system such as the one in equation (20), characterized by red-noise-like spectral features and “short-memory”, the coupling propagates along all the scales in a homogeneous way. To better highlight possible asymmetries in the coupling at different temporal scales s and the variability in asymmetry across the diverse simulations of the ensemble, we also extracted the minimum correlation $r_{min} = \min \{r_{s,\tau}\}_{\tau=-k}^k$ for each single realization and derived the ensemble minimum mean $\bar{r}_{min} = E[r_{min}]$ and standard deviation $\sigma_{r_{min}}$. The focus is here on the minimum of $r_{s,\tau}$ since the two synthetic systems are negatively coupled. However similar considerations on the scale-by-scale maximum of $r_{s,\tau}$ could be done in the case of a positively correlated process. As discussed next, \bar{r}_{min} and $\sigma_{r_{min}}$ provide a rough estimate of the asymmetry and variability of peak correlations in the analyzed system.

In Figure 3a-b,d, \bar{r}_{min} (black empty circles) and its confidence interval at the 99% significance level (bounded by the blue and red solid lines) were overlapped to the $r_{s,\tau}$ diagram to show how the peak correlation moves from one side to the other of the 0 bisecting line when the coupling direction is inverted. Top panels in Figure 3 also show the fast – quasi exponential – oscillatory decay of $r_{s,\tau}$ at different scales s , typical of the lagged-cross correlation of an absolutely integrable signal. Depending on the scale, this oscillation decays below the $\alpha = 99\%$ significance level more (fine-scales) or less (coarse scales) rapidly, consistently with the fact that the memory of the process is in general weaker at finer scales. We also test the ability of $r_{s,\tau}$ for identifying null-coupling across-scales by posing $C_1 = C_2 = 0$ in equation (20). The wavelet cross-correlation patterns obtained from a single-realization of the uncoupled system are shown in Figure 3c, while panel d depicts the corresponding ensemble statistic. As evident the ensemble $r_{s,\tau}$ in

Figure 3d never passes the test for the non-null correlation and can robustly detect the lack of coupling across scales. Also, \bar{r}_{\min} oscillates around $\tau = 0$ with strong variability at all scales.

Figure 3e finally shows the distribution of the minimum value of the $r_{s,\tau}$ at two selected scales, i.e. 10 and 120 samples, in the case when both coupling and direction are set to vary. Also here, the confidence intervals of \bar{r}_{\min} are computed from an ensemble of 100 realizations of the VAR(1) at the level of 99%. Panel e shows that for a sufficient strong value of the coupling, \bar{r}_{\min} can effectively capture the switch in directionality of the coupling at both sample scales. At larger scale (120 samples) however, while the value of \bar{r}_{\min} is higher than for the smaller scale (10 samples), the variability is also higher. For any value of the coupling parameter falling in the interval $[C_1 > -0.2, C_2 > -0.2]$ the estimated range of variability of \bar{r}_{\min} ends up crossing the zero lag axis and thus does not provide a valid estimate of the directionality of the process. Therefore, the weaker the coupling, the larger the uncertainty on the actual directionality. In addition, uncertainty increases with scale due to the higher redundancy of wavelet coefficients.

3.2. Coupling in a Second-Order Vector Auto-regressive System with Localized Pseudo-periodicity

In this section we test the capability of $r_{s,\tau}$ in detecting couplings that are well-localized in frequency – i.e. occurring at a specific time-scale. The ability to resolve such localized correlations is important to the study of environmental systems, which often display strong sub-seasonal, seasonal and inter-annual oscillations. To do so, we consider the following second order vector autoregressive model (VAR(2)) where a *pseudo-periodic coupling* from

y to x is imposed by choosing roots close to the unit circle:

$$\begin{bmatrix} x_t \\ y_t \end{bmatrix} = \begin{bmatrix} 0.55 & 0.00 \\ 0.00 & 0.55 \end{bmatrix} \begin{bmatrix} x_{t-1} \\ y_{t-1} \end{bmatrix} + \begin{bmatrix} -0.80 & -0.30 \\ 0.00 & -0.80 \end{bmatrix} \begin{bmatrix} x_{t-2} \\ y_{t-2} \end{bmatrix} + \begin{bmatrix} \epsilon_t \\ \xi_t \end{bmatrix}. \quad (21)$$

A similar system is used in *Dhamala et al.* [2008b] in the context of spectral Granger causality metrics. Given the localization in frequency of the simulated coupling, the system in equation (21) is additionally used to demonstrate the role of wavelet localization in the efficient estimation of $r_{s,\tau}$.

Top panels in Figure 4 show $r_{s,\tau}$ as estimated from an ensemble of 100 realizations of equation (21), and by respectively using the Morlet (a) and Paul (b) wavelets. Both plots only display values above the $\alpha = 99\%$ significance level, and they both show the confidence interval (always 99%) for \bar{r}_{\min} averaged over the 100 realizations. Panel c reports the theoretical power spectra of each of the x and y autoregressive sub-spaces displaying a clear periodicity at $1/5$ of the cycle. Figure 4a-b clearly show that the $r_{s,\tau}$ obtained through the Morlet wavelet better identifies the frequency peak of the coupling in agreement with the characteristics of the kernel, that is by construction, more localized in frequency. In contrast, the frequency peak in the Paul $r_{s,\tau}$ results more spread out, especially in the range of lower scales, but better resolved in time.

Nonetheless, both the Paul and the Morlet $r_{s,\tau}$ are able to correctly detect the directionality ($y \rightarrow x$), as evident in the left-asymmetry of \bar{r}_{\min} . It is also worth noting that the variability of \bar{r}_{\min} is lower where the coupling is stronger (around the frequency peak), gradually increasing with the scale. This is mainly due to the size and relative higher overlapping of the wavelets at larger temporal scales. In summary, both the Morlet and the Paul wavelet cross-correlations are able to extract the essential features of the coupling.

The choice between the two different wavelets should be made based on the application and the characteristics of the signals under investigation.

3.3. Fast/Slow Dynamics Separation and Feedback

In section 1 we argue that the evolution of geophysical systems often results from the interaction of diverse dynamical scales. A simple example can be provided by a coupling-feedback system in which the forcing is acting at shorter temporal scales than the response – i.e. a fast/slow dynamical system. In such a case, classic correlation analysis in the time domain fails unless the strength of the coupling in one of the two directions is dominant. The wavelet cross-correlation, in contrast, can still resolve the two components of the coupling, their asymmetry and characteristic scales. Let us consider a modification of the VAR(2) system in equation (21) in which x is driving y (negative correlation) at a frequency of 1/15 of cycle (f_{slow}) and y is forcing x (positive correlation) around the 1/6 of cycle (f_{fast}):

$$\begin{bmatrix} x_t \\ y_t \end{bmatrix} = \begin{bmatrix} 1.73 & 0.00 \\ 0.00 & 0.85 \end{bmatrix} \begin{bmatrix} x_{t-1} \\ y_{t-1} \end{bmatrix} + \begin{bmatrix} -0.90 & -0.10 \\ 0.30 & -0.95 \end{bmatrix} \begin{bmatrix} x_{t-2} \\ y_{t-2} \end{bmatrix} + \begin{bmatrix} \epsilon_t \\ \xi_t \end{bmatrix}. \quad (22)$$

The corresponding $r_{s,\tau}$ estimated by using both the Morlet and the Paul wavelets is shown in Figure 5, together with the normalized spectra of the two variables. It is evident that also in this case, the $r_{s,\tau}$ is able to resolve the scales at which the coupling actually take place, as well as the opposite asymmetry of the correlation at these scales. In this case the \bar{r}_{min} is only representative of the coupling from x to y due to the negative linear correlation among the two variable at f_{slow} . However, mainly as a consequence of the strong periodicity of the coefficients at both the forcing and feedback scales, the localization of \bar{r}_{min} is also at some extent representative of the asymmetry in the coupling

from y to x . This is overall an interesting result considering that interactions characterized by different degrees of “memory” and fluctuation-response relaxation (FRR) effects are ubiquitous in geosciences [*Lacorata and Vulpiani*, 2007; *Leith*, 1975].

4. Multiscale Interactions in the Soil Moisture-Temperature Coupling

Land-atmosphere interactions, their strength and directionality, are one of the main sources of uncertainty in current climate models with strong implications for the accurate assessment of future climate change impacts at regional scales [see e.g. *Seneviratne et al.*, 2010]. Besides the scarcity of direct observations of the states and fluxes across the land-atmosphere continuum, major uncertainties originate from the inherent complexity in the way these variables interact, the multiscale character of these interactions, and the existence of critical tipping points in water and energy availability that may trigger regime transitions. In this last section, we apply the wavelet cross-correlation analysis to a classic form of interaction between land and atmosphere: the coupling between soil moisture (θ) and near-surface air temperature (T).

The objective is to isolate the different components of the coupling across a wide range of temporal scales (from fine weather scales to seasonal to inter-annual) and considering different lag-times between the variables. These two variables (θ , T) are mainly related through the process of latent heat flux. They are a priori negatively correlated; however, their coupling can occur in both directions: (a) T may regulate θ via the drying of the soil due to evaporation, or (b) θ may regulate T due to evaporative cooling [*Seneviratne et al.*, 2010; *Miralles et al.*, 2012; *Mueller and Seneviratne*, 2012]. The latter feedback of θ on T occurs in regions that are water-limited and it has been referred as a reason

why droughts and heatwaves coexist, or follow one another [Quesada *et al.*, 2012; Miralles *et al.*, 2014].

Nonetheless, the mechanisms through which different dynamical scales contribute to the onset and persistence of the θ - T coupling and feedback remain unclear to a large extent [Orlowsky and Seneviratne, 2010]. In this study we use estimates of daily maximum air temperature obtained from the sub daily screen level (2 m) temperatures of ERA-Interim (http://apps.ecmwf.int/datasets/data/interim_full_daily/) the most recent climate reanalysis product of the European Center for Medium Range Weather Forecasts (ECMWF) [Dee *et al.*, 2011]. We consider temperature fields for the period 1980-2011 over a global grid with a spatial resolution of 0.75 degrees, corresponding to the native reduced Gaussian grid of ERA [Berrisford *et al.*, 2011; Simmons *et al.*, 2014]. Temporal resolution of the assimilated and predicted fields (i.e. the analysis fields) we use here is 6 hours. We extract and analyze maximum daily temperatures as they are most strongly impacted by soil moisture deficits and evaporative cooling effects [Orlowsky and Seneviratne, 2010; Mueller and Seneviratne, 2012]. It is important to note that ERA-Interim temperature is constrained by observations through a complex 4-D assimilation process [Dee *et al.*, 2011]. As a consequence the quality of the analyzed fields is strongly dependent on the density of the station network in the region under consideration [see Simmons, 2011]. However, the main advantage of reanalysis over direct observations and classical interpolation schemes is their ability to combine observations with a physical model of the atmosphere able to produce physically coherent high-resolution fields and propagate information to areas with poor observational coverage. For θ we use an independent data source, the global daily root-zone soil moisture estimates from GLEAM (Global Land-surface Evaporation:

the Amsterdam Methodology – <http://foofoo.ugent.be/satex/GLEAM/> as described in *Miralles et al.* [2012, 2011a, b, 2013], also for the period 1980-2011. GLEAM is a set of algorithms designed to retrieve information on evaporation from current satellite observations of hydro-climatic variables [*Miralles et al.*, 2013]. In GLEAM, θ is derived at daily timescales through the assimilation of satellite soil moisture observations into a multi-layer running water balance that reproduces the infiltration of rainfall through the vertical soil profile [*Owe et al.*, 2008].

Figure 6 shows the results of the wavelet cross-correlation analysis for different geographical locations, spanning a wide range of diverse climatic regimes. From top to bottom the panels are ordered by decreasing level of aridity. The panels in the right column show the exact geographical location of the grid points used in the analysis. Wavelet cross-correlations $r_{s,\tau}$ in Figure 6 represent the coupling between T and θ at a later time, so that T drives θ if $r_{s,\tau}$ is significant at negative lags and vice versa, θ drives T for positive lags. The $r_{s,\tau}$ is estimated based on a Paul kernel with $m = 4$, as an ensemble metric across the available range of years (1980-2011). The resulting correlation patterns can therefore be interpreted as *ensemble averages* of the θ - T coupling across scales. We use here the Paul wavelet based on its superior performance in resolving temporal variability. However, substantially similar results were obtained by using the Morlet kernel. At each location in space, $r_{s,\tau}$ is computed for the entire annual cycle (left panels), only Boreal summer (MJJA, central panels) and only Boreal winter (NDJF, right panels). Before inferring $r_{s,\tau}$, time-series of both T and θ are normalized to have zero mean and unit variance. Therefore, harmonic and persistent oscillations are preserved, i.e. we are not

specifically analyzing seasonally de-trended anomalies, as one of the main goals is in fact to isolate the relative role of different harmonic components.

As the expected correlation between T and θ is mostly negative, the minimum correlation (\bar{r}_{min}) and its confidence interval can represent a proxy of temporal asymmetry in the multiscale coupling also in this case. The confidence interval of the ensemble seasonal $r_{s,\tau}$ (winter or summer) are computed by considering each summer (or winter) as single time series, resulting in 24 annual realizations. For the full time series in contrast, the confidence interval is calculated by using a sliding window approach. At each step, $r_{s,\tau}$ is estimated over a time-window of 5 years, sliding forward with a 1 year time step. The maximum scale at which $r_{s,\tau}$ can be inferred in the annual and seasonal cases is limited by the size of each sample. Therefore we do not consider any periodicity larger than three months for seasonal samples since this modes are only partially sampled in the data.

Panels a-c show $r_{s,\tau}$ for a location in central Sahara for the full time series (a), MJJA (b), and NDJF (c). Here, the extreme dryness of the soil is expected to inhibit coupling; consequently, a significant correlation can only be found for T driving θ at the annual scale (circa 360 days) (see Figure 6a). This coupling, however, is mostly related to the seasonal cycle of temperature since in a hot desert climate, soil moisture retrievals mostly resemble a white noise signal and sensible heat dominates the exchange of energy between land and atmosphere. The extremely erratic behavior of the soil water content is captured by the symmetry of the minimum \bar{r}_{min} (absence of directionality in the coupling) and by the large variability in its confidence interval (Figure 6a). Therefore, hot and dry desert climates can be seen here as a test for null directional coupling across scales, similarly to the synthetic case study reported in Figure 3c-d.

Correlation patterns radically change when we move to a location within the Sahelian sub-region of Mali (Figure 6d-f). In this case most of the precipitation (200-400 mm) falls during the summer months (MJJA), but it is sufficient to trigger the coupling between soil moisture and temperature across a wide range of temporal scales spanning a few days to months (Figure 6d,e). In contrast, the coupling disappears during the winter months (Figure 6f) due to soil desiccation. The seasonally dry character of this climate is captured by the second harmonic at half a year (around 180 days). During the entire year (6d), T leads θ at time scales of one to 6 months, and θ leads T at longer time scales. An analogous pattern can also be identified in Northwestern Australia (Figure 6g-i), another seasonally dry location with a similar separation between humid and water-limited regimes. During Austral summer (NDJF), significant correlations are still confined to the negative lags half-quadrant - i.e. in average, T drives θ through evaporation – although the small scales (few days to 1 month) are clearly the most variable in terms of asymmetry of the coupling.

This fact could be connected with a higher occurrence of θ feedbacks on T at these scales throughout the twenty-one years of the ensemble (Figure 6e). Compared to Mali (Figure 6d), the variability of \bar{r}_{min} , and consequently the uncertainty on directionality, is here less pronounced, i.e. the members in the ensemble (g and i) follow very similar correlation patterns at both small and large scales. During the rainy season (Austral winter, Figure 6h) θ is not limiting evaporation, while during the summer the coupling extends throughout a wide range of scales (Figure 6i), with significant correlations also at positive lags (θ leading T) and at the finest scales [Dirmeyer, 2011; Miralles *et al.*, 2012].

The separation between water-limited and *wet* regime is also present in the wavelet cross-correlation patterns of a temperate mid-latitude location in central France (Figure

6j-l). During all year (6j), the coupling is present at larger scales (> 90 days), and stronger for T leading θ than θ leading T . During the summer months (6k), negative correlations are found for negative lags, similar to the results for Mali (6i and 6e) and indicating an influence of T on θ at all timescales. On the other hand, during the winter (6l), θ leads T at large scales. The confidence interval or \bar{r}_{min} , however, mostly falls into null correlation regions and thus points to some uncertainties in these results. In general, the seasonal separation is weaker than in Mali (6e and f) and Northwestern Australia (6h and i). Finally, a site located not far from the coast of Gabon is displayed in Figure 6m-o. The site is characterized by a tropical climate and strong moisture advection from the Ocean, hence θ does not represent a limiting factor in this case, and the only (positive) observed correlation is the one derived from the synchronization between the seasonal cycle of temperature and precipitation in the region [see e.g., *Zhou et al.*, 2014]. Overall the wavelet cross-correlation $r_{s,\tau}$ is able to capture the scale-by-scale strength and directionality of the θ - T coupling across different climatic regimes in a consistent way. Moreover, it allows the separation of the local scale contribution from the seasonal signal - often dominant in time domain statistics. Correlation results are stronger in transitional regimes, consistent with previous studies [*Koster et al.*, 2004; *Seneviratne and Koster*, 2012; *Miralles et al.*, 2012], and interestingly, the θ - T coupling propagates across all the analyzed scales during the warm season, when land-atmospheric interactions may be critical for high temperature extremes [*Seneviratne et al.*, 2006; *Quesada et al.*, 2012; *Miralles et al.*, 2014].

5. Conclusions

We introduced a novel methodology to infer multiscale interactions from observations of dynamical systems that evolve over diverse temporal scales. The here adopted metric

– the wavelet cross-correlation $r_{s,\tau}$ – is based on the direct estimation of scale-by-scale correlations in the wavelet domain. The ability of $r_{s,\tau}$ to infer interactions across scales – and their directionality – was tested on different synthetic coupled systems and on a real-world case study of land-atmosphere interaction the coupling/feedback between soil moisture and near-surface air temperature. When applied to bi-variate auto-regressive vector models of increasing complexity the $r_{s,\tau}$ shows to be able to correctly reproduce the underlying directionality of the coupling at different temporal scales, and to distinguish fast/slow dynamic components within the simulated systems. In this context the term directionality is mainly used to indicate some sort of temporally lagged coupling at the considered scale, without any assumption on the causal structure of the observed process.

However, it is clear that the ability of decomposing a coupling in its scale-by-scale components is an attractive feature of wavelet cross-correlation and can be used in disentangle the role of different dynamical processes in coupled geophysical systems. Besides directionality is here mainly a synonymous for temporal asymmetry, and connections between causality and predictability – like in the case of more proper causality metrics like Granger causality [*Granger*, 1969] – were not yet explored.

The application of wavelet cross-correlations to soil moisture and near surface air temperature shows interesting insights into the interaction of these two variables at different climate regimes. An interesting feature of this interaction, when observed through the lens of a multiscale correlation metrics like $r_{s,\tau}$, is that the coupling between soil moisture and temperature, in the passage to a water limited regime, is active through an extremely wide range of scales, and that this feature represents a common signature of the coupling (and possible feedback) across very diverse climatic regimes. An interesting

question arising from this evidence could be whether this activation of the coupling across scales is a feature reproducible in climate models. A word of caution is finally in order when we consider couplings taking place at large temporal scales (> 1 year), since they could be partially affected by the redundancy – and consequent auto-correlation effects – of the continuous wavelet transform. Overall results of this study demonstrate the potential of wavelet cross-correlations to unravel the relationships between two environmental and climatic variables from a purely statistical perspective. The method here described can, in principle, be applied to observations from any region of the world, and to study soil moisture-temperature coupling or any other multivariate interaction across multiple scales.

Acknowledgments. The data used in this manuscript are publicly available from the ERA Interim (http://apps.ecmwf.int/datasets/data/interim_full_daily/) and GLEAM (<http://foofoo.ugent.be/satex/GLEAM/>) online repositories.

E. Casagrande, D. Entekhabi and A. Molini thankfully acknowledge the funding from Masdar Institute (One-to-One MIT-MI, #12WAMA1) in the framework of the MIT and Masdar Institute Cooperative Program.

References

- Agnew, D. C. (1992), The time-domain behavior of power-law noises, *Geophys. Res. Lett.*, *19*(4), 333–336.
- Allen, C. R., and C. S. Holling (2002), Cross-scale Structure and Scale Breaks in Ecosystems and Other Complex Systems, *Ecosystems*, *5*(4), 315–318.
- Allen, C. R., and C. S. Holling (2013), *Discontinuities in Ecosystems and Other Complex Systems*, Columbia University Press, New York, USA.
- Arneodo, A., J. F. Muzy, and D. Sornette (1998), “Direct” causal cascade in the stock market, *Eur. Phys. J. B*, *2*, 277–282.
- Berrisford, P., D. Dee, P. Poli, R. Brugge, K. Fielding, M. Fuentes, P. Kallberg, S. Kobayashi, S. Uppala, and A. Simmons (2011), The ERA-Interim Archive – Version 2.0, *Tech. Rep. ERA report series 1, Technical Report. ECMWF*, Reading, UK.
- Bettencourt, L. M. A., J. Lobo, D. Helbing, C. Kühnert, and G. B. West (2007), Growth, innovation, scaling, and the pace of life in cities., *P. Natl. Acad. Sci. USA*, *104*(17), 7301–7306.
- Cash, D. W., W. N. Adger, F. Berkes, P. Garden, L. Lebel, P. Olsson, L. Pritchard, and O. Young (2006), Scale and cross-scale dynamics: governance and information in a multilevel world, *Ecol. Soc.*, *11*(2), 8.
- Chen, Y., and Y. Zhou (2008), Scaling laws and indications of self-organized criticality in urban systems, *Chaos, Solitons & Fractals*, *35*(1), 85–98.
- Cowen, R. K., C. B. Paris, and A. Srinivasan (2006), Scaling of connectivity in marine populations., *Science*, *311*(5760), 522–527.

- Crowley, P. M. (2007), A Guide to Wavelets for Economists, *J. Econ. Surv.*, *21*(2), 207–267.
- Daubechies, I. (1992), *Ten lectures on wavelets*, SIAM - Society of Applied and Industrial mathematics, Philadelphia, USA.
- Debra P. C. Peters, R. A. Pielke Sr, B. T. Bestelmeyer, C. D. Allen, S. Munson-McGee, and K. M. Havstad (2007), Spatial Nonlinearities: Cascading Effects in the Earth System, in *Terrestrial Ecosystems in a Changing World*, pp. 165–174, Springer Berlin-Heidelberg, Berlin, Germany.
- Dee, D. P., S. M. Uppala, A. J. Simmons, P. Berrisford, P. Poli, S. Kobayashi, U. Andrae, M. A. Balmaseda, G. Balsamo, P. Bauer, P. Bechtold, A. C. M. Beljaars, L. van de Berg, J. Bidlot, N. Bormann, C. Delsol, R. Dragani, M. Fuentes, A. J. Geer, L. Haimberger, S. B. Healy, H. Hersbach, E. V. Hólm, L. Isaksen, P. Kållberg, M. Köhler, M. Matricardi, A. P. McNally, B. M. Monge-Sanz, J. J. Morcrette, B. K. Park, C. Peubey, P. de Rosnay, C. Tavalato, J. N. Thépaut, and F. Vitart (2011), The ERA-Interim reanalysis: configuration and performance of the data assimilation system, *Q. J. R. Meteorol. Soc.*, *137*(656), 553–597.
- Dhamala, M., G. Rangarajan, and M. Ding (2008a), Analyzing information flow in brain networks with nonparametric Granger causality, *NeuroImage*, *41*(2), 354–362.
- Dhamala, M., G. Rangarajan, and M. Ding (2008b), Estimating Granger causality from fourier and wavelet transforms of time series data., *Phys. Rev. Lett.*, *100*(1), 018701.
- Dirmeyer, P. A. (2011), The terrestrial segment of soil moisture-climate coupling, *Geophys. Res. Lett.*, *38*(1), L16702.

- Edgell, S. E., and S. M. Noon (1984), Effect of violation of normality on the t -test of the correlation coefficient, *Psychol. Bull.*, *95*(3), 576–583.
- Fisher, R. A. (1915), Frequency distribution of the values of the correlation coefficient in samples from an indefinitely large population, *Biometrika*, *10*(4), 507–521.
- Foufoula-Georgiou, E., and P. Kumar (1994), *Wavelets in Geophysics*, Wavelet Analysis and Its Applications, v.4, Academic Press, San Diego, USA.
- Frisch, U., and A. N. Kolmogorov (1995), *Turbulence*, The Legacy of A. N. Kolmogorov, Cambridge University Press, New York, USA.
- Gençay, R., F. Selçuk, and B. J. Whitcher (2001), *An Introduction to Wavelets and Other Filtering Methods in Finance and Economics*, Academic Press, San Diego, USA.
- Granger, C. W. J. (1969), Investigating Causal Relations by Econometric Models and Cross-spectral Methods, *Econometrica*, *37*(3), 424.
- Grinsted, A., J. C. Moore, and S. Jevrejeva (2004), Application of the cross wavelet transform and wavelet coherence to geophysical time series, *Nonlinear Proc. Geoph.*, *11*(5-6), 561–566.
- Guttal, V., and C. Jayaprakash (2009), Spatial variance and spatial skewness: leading indicators of regime shifts in spatial ecological systems, *Theor. Ecol.*, *2*(1), 3–12.
- Havlicek, L. L., and N. L. Peterson (1977), Effect of the violation of assumptions upon significance levels of the Pearson r , *Psychol. Bull.*, *84*(2), 373–377.
- Hirschi, M., S. I. Seneviratne, V. Alexandrov, F. Boberg, C. Boroneant, O. B. Christensen, H. Formayer, B. Orlowsky, and P. Stepanek (2010), Observational evidence for soil-moisture impact on hot extremes in southeastern Europe, *Nature*, *4*(1), 17–21.

- Holbrook, N. J., J. Li, M. Collins, E. Di Lorenzo, F.-F. Jin, T. Knutson, M. Latif, C. Li, S. B. Power, R. Huang, and G. Wu (2014), Decadal Climate Variability and Cross-Scale Interactions: ICCL 2013 Expert Assessment Workshop, *BAMS*, *95*(8), 155–ES158.
- Johnson, N. L., S. Kotz, and N. Balakrishnan (1994), *Continuous univariate distributions*, vol. 2, Wiley-Interscience, New York, USA.
- Kendall, M. G., and A. Stuart (1945), *The Advanced theory of statistics*, vol. I, London, UK.
- Keshner, M. S. (1982), 1/f noise, *Proceedings of the IEEE*, *70*(3), 212–218.
- Koster, R. D., P. A. Dirmeyer, Z. C. Guo, G. Bonan, E. Chan, P. Cox, C. T. Gordon, S. Kanae, E. Kowalczyk, D. Lawrence, P. Liu, C. H. Lu, S. Malyshev, B. McAvaney, K. Mitchell, D. Mocko, T. Oki, K. Oleson, A. Pitman, Y. C. Sud, C. M. Taylor, D. Verseghy, R. Vasic, Y. K. Xue, T. Yamada, and G. Team (2004), Regions of strong coupling between soil moisture and precipitation, *Science*, *305*(5687), 1138–1140.
- Kumar, P., and E. Foufoula-Georgiou (1997), Wavelet analysis for geophysical applications, *Rev. Geophys.*, *35*(4), 385–412.
- Lacorata, G., and A. Vulpiani (2007), Fluctuation-Response Relation and modeling in systems with fast and slow dynamics, *Nonlinear Proc. Geoph.*, *14*(5), 681–694.
- Lämmer, S., B. Gehlsen, and D. Helbing (2006), Scaling laws in the spatial structure of urban road networks, *Physica A*, *363*(1), 89–95.
- Leith, C. E. (1975), Climate Response and Fluctuation Dissipation., *J. Atmos. Sci.*, *32*(1), 2022–2026.
- Li, H., and T. Nozaki (1997), Application of Wavelet Cross-Correlation Analysis to a Plane Turbulent Jet., *JSME Int. J. B-Fluid T.*, *40*(1), 58–66.

- Lovejoy, S., and D. Schertzer (2013), *The Weather and Climate: Emergent Laws and Multifractal Cascades*, Cambridge University Press, Cambridge, UK.
- Lungarella, M., A. Pitti, and Y. Kuniyoshi (2007), Information transfer at multiple scales, *Phys. Rev. E*, *76*(5), 056117.
- Lux, T., and M. Marchesi (1999), Scaling and criticality in a stochastic multi-agent model of a financial market, *Nature*, *397*(6719), 498–500.
- Mallat, S. (2008), *A Wavelet Tour of Signal Processing, The Sparse Way*, Academic Press, San Diego, USA.
- Mandelbrot, B. B. (1997), *Fractals and Scaling In Finance*, Discontinuity, Concentration, Risk, Springer, New York, USA.
- Mandelbrot, B. B., and I. Stewart (1998), Fractals and scaling in finance, *Nature*, *391*(6669), 758–758.
- Maraun, D., and J. Kurths (2004), Cross wavelet analysis: significance testing and pitfalls, *Nonlinear Proc. Geoph.*, *11*(4), 505–514.
- Maraun, D., J. Kurths, and M. Holschneider (2007), Nonstationary Gaussian processes in wavelet domain: synthesis, estimation, and significance testing., *Phys. Rev. E*, *75*(1 Pt 2), 016707.
- Miralles, D. G., T. R. H. Holmes, R. A. M. De Jeu, J. H. Gash, A. G. C. A. Meesters, and A. J. Dolman (2011a), Global land-surface evaporation estimated from satellite-based observations, *Hydrol. Earth Syst. Sc.*, *15*, 453–469.
- Miralles, D. G., R. A. M. De Jeu, J. H. Gash, T. R. H. Holmes, and A. J. Dolman (2011b), Magnitude and variability of land evaporation and its components at the global scale, *Hydrol. Earth Syst. Sc.*, *15*, 967–981.

- Miralles, D. G., M. J. van den Berg, A. J. Teuling, and R. A. M. de Jeu (2012), Soil moisture-temperature coupling: A multiscale observational analysis, *Geophys. Res. Lett.*, *39*(2), L21707.
- Miralles, D. G., M. J. van den Berg, J. H. Gash, R. M. Parinussa, R. A. M. de Jeu, H. E. Beck, T. R. H. Holmes, C. Jiménez, N. E. C. Verhoest, W. A. Dorigo, A. J. Teuling, and A. Johannes Dolman (2013), El Niño–La Niña cycle and recent trends in continental evaporation, *Nature Climate Change*, *4*(2), 122–126.
- Miralles, D. G., A. J. Teuling, C. C. van Heerwaarden, and J. V.-G. de Arellano (2014), Mega-heatwave temperatures due to combined soil desiccation and atmospheric heat accumulation, *Nature Geoscience*, *7*(5), 345–349.
- Mizuno-Matsumoto, Y., T. Yoshimine, Y. Nii, A. Kato, M. Taniguchi, J. K. Lee, T. S. Ko, S. Date, S. Tamura, S. Shimojo, K. Shinosaki, T. Inouye, and M. Takeda (2001), Landau-Kleffner Syndrome: Localization of Epileptogenic Lesion Using Wavelet- Cross-Correlation Analysis., *Epilepsy Behav.*, *2*(3), 288–294.
- Moilanen, A., and M. Nieminen (2002), Simple Connectivity Measures in Spatial Ecology, *Ecology*, *83*(4), 1131.
- Molini, A., G. G. Katul, and A. Porporato (2010a), Causality across rainfall time scales revealed by continuous wavelet transforms, *J. Geophys. Res. Atmos.*, *115*(D14), D14123.
- Molini, A., G. G. Katul, and A. Porporato (2010b), Scale-wise evolution of rainfall probability density functions fingerprints the rainfall generation mechanism, *Geophys. Res. Lett.*, *37*(7), L07403.
- Moritz, M. A., M. E. Morais, L. A. Summerell, J. M. Carlson, and J. Doyle (2005), Wild-fires, complexity, and highly optimized tolerance., *P. Natl. Acad. Sci. USA*, *102*(50),

17,912–17,917.

Mueller, B., and S. I. Seneviratne (2012), Hot days induced by precipitation deficits at the global scale, *P Natl. Acad. Sci. USA*, *109*(31), 12,398–12,403.

Muzzy, J. F., E. Bacry, and A. Arneodo (2011), The Multifractal Formalism Revised with Wavelets, *Int. J. Bifurcat. Chaos*, *4*(2), 245–302.

Nagelkerken, I. (2009), *Ecological Connectivity among Tropical Coastal Ecosystems*, Springer Science & Business Media, Dordrecht, The Netherlands.

Ngae, P., M. Grignon, and J.-G. Poloniecki (1998), Détermination d’une vitesse de convection à partir de la décomposition en ondelettes d’un champ thermique, *Int. J. Therm. Sci.*, *38*(4), 331–339.

Nikkinen, J., S. Pynnönen, M. Ranta, and S. Vähämaa (2011), Cross-dynamics of exchange rate expectations: a wavelet analysis, *Int. J. Financ. Econ.*, *16*(3), 205–217.

Ódor, G. (2013), Spectral analysis and slow spreading dynamics on complex networks, *Phys. Rev. E*, *88*(3), 032109.

Okin, G. S., A. J. Parsons, J. Wainwright, J. E. Herrick, B. T. Bestelmeyer, D. C. Peters, and E. L. Fredrickson (2009), Do Changes in Connectivity Explain Desertification?, *BioScience*, *59*(3), 237–244.

Onorato, M., M. V. Salvetti, and G. Buresti (1997), Application of a wavelet cross-correlation analysis to DNS velocity signals, *Eur. J. Mech., B/Fluids*, *16*, 575–597.

Orlowsky, B., and S. I. Seneviratne (2010), Statistical Analyses of Land-Atmosphere Feedbacks and Their Possible Pitfalls, *J. Climate*, *23*(14), 3918–3932.

Owe, M., R. de Jeu, and T. Holmes (2008), Multisensor historical climatology of satellite-derived global land surface moisture, *J Geophys. Res. Earth*, *113*(F1), F01002.

- Pastor-Satorras, R., and A. Vespignani (2001), Epidemic Spreading in Scale-Free Networks, *Phys. Rev. Lett.*, *86*(14), 3200–3203.
- Percival, D. B. (1999), Wavelet-based surrogates for testing time series, in *Proceedings of the First Joint BMES/EMBS Conference (BMEEMB-99)*, vol. 2, p. 910, IEEE.
- Percival, D. B., and H. O. Mofjeld (1997), Analysis of Subtidal Coastal Sea Level Fluctuations Using Wavelets, *J. Am. Stat. Assoc.*, *92*(439), 868–880.
- Peters, D., B. Bestelmeyer, and M. Turner (2007), Cross-Scale Interactions and Changing Pattern–Process Relationships: Consequences for System Dynamics, *Ecosystems*, *10*(5), 790–796.
- Peters, Debra P. C., R. A. Pielke, B. T. Bestelmeyer, C. D. Allen, S. Munson-McGee, and K. M. Havstad (2004), Cross-scale interactions, nonlinearities, and forecasting catastrophic events., pp. 15,130–15,135.
- Pumain, D. (2004), Scaling laws and urban systems, *SFI Working Paper*, pp. 2004–02–002.
- Quesada, B., R. Vautard, P. Yiou, M. Hirschi, and S. I. Seneviratne (2012), Asymmetric European summer heat predictability from wet and dry southern winters and springs, *Nature Climate Change*, *2*(10), 736–741.
- Raffa, K. F., B. H. Aukema, B. J. Bentz, A. L. Carroll, J. A. Hicke, M. G. Turner, and W. H. Romme (2008), Cross-scale Drivers of Natural Disturbances Prone to Anthropogenic Amplification: The Dynamics of Bark Beetle Eruptions, *BioScience*, *58*(6), 501–517.
- Rial, J. A., R. A. Pielke Sr, M. Beniston, M. Claussen, J. Canadell, P. Cox, H. Held, N. de Noblet-Ducoudré, R. Prinn, J. F. Reynolds, and J. D. Salas (2004), Nonlinearities, Feedbacks and Critical Thresholds within the Earth’s Climate System, *Climatic Change*,

65(1-2), 11–38.

Salvetti, M. V., F. Beux, and G. Lombardi (1999), Application of a Wavelet Cross-Correlation Technique to the Analysis of Mixing, *AIAA Journal*, 37(8), 1007–1010.

Scanlon, T. M., K. K. Caylor, S. A. Levin, and I. Rodriguez-Iturbe (2007), Positive feedbacks promote power-law clustering of Kalahari vegetation, *Nature*, 449(7159), 209–212.

Schmitt, F. G., and P. Chainais (2007), On causal stochastic equations for log-stable multiplicative cascades, *Eur. Phys. J. B*, 58(2), 149–158.

Sello, S., and J. Bellazzini (2000), Wavelet Cross-Correlation Analysis of Turbulent Mixing from Large-Eddy-Simulations, *arXiv:physics/0003029v1*, p. 3029.

Seneviratne, S. I., and R. D. Koster (2012), A Revised Framework for Analyzing Soil Moisture Memory in Climate Data: Derivation and Interpretation, *Journal of Hydrometeorology*, 13(1), 404–412.

Seneviratne, S. I., D. Lüthi, M. Litschi, and C. Schär (2006), Land–atmosphere coupling and climate change in Europe, *Nature*, 443(7108), 205–209.

Seneviratne, S. I., T. Corti, E. L. Davin, M. Hirschi, E. B. Jaeger, I. Lehner, B. Orlowsky, and A. J. Teuling (2010), Investigating soil moisture–climate interactions in a changing climate: A review, *Earth-Sci. Rev.*, 99(3-4), 125–161.

Shirazi, A. H., C. Aghamohammadi, M. Anvari, A. Bahraminasab, M. R. Rahimi Tabar, J. Peinke, M. Sahimi, and M. Marsili (2013), Scale dependence of the directional relationships between coupled time series, *J. Stat. Mech.*, 2, P02042.

Simmons, A. (2011), From observations to service delivery: Challenges and opportunities, *WMO Bulletin*, 60(2).

- Simmons, A. J., P. Poli, D. P. Dee, P. Berrisford, H. Hersbach, S. Kobayashi, and C. Peubey (2014), Estimating low-frequency variability and trends in atmospheric temperature using ERA-Interim, *Q. J. R. Meteorol. Soc.*, *140*(679), 329–353.
- Solé, R. V., S. C. Manrubia, M. Benton, S. Kauffman, and P. Bak (1998), Criticality and scaling in evolutionary ecology, *Trends Ecol. Evol.*, *14*(4), 156–160.
- Szell, M., R. Lambiotte, and S. Thurner (2010), Multirelational organization of large-scale social networks in an online world., *P. Natl. Acad. Sci. USA*, *107*(31), 13,636–13,641.
- Thrush, S. F., J. E. Hewitt, A. M. Lohrer, and L. D. Chiaroni (2013), When small changes matter: the role of cross-scale interactions between habitat and ecological connectivity in recovery, *Ecol. Appl.*, *23*(1), 226–238.
- Torrence, C., and G. P. Compo (1998), A practical guide to wavelet analysis, *B. Am. Meteorol. Soc.*, *79*(1), 61–78.
- Torrence, C., and P. J. Webster (1999), Interdecadal changes in the ENSO-monsoon system, *J. Climate*, *12*(8), 2679–2690.
- Tsonis, A. A., and J. B. Elsner (2007), *Nonlinear Dynamics in Geosciences*, Springer Science & Business Media, Dordrecht, The Netherlands.
- Turbelin, G., P. Ngae, and M. Grignon (2008), Wavelet cross-correlation analysis of wind speed series generated by ANN based models, *Renew. Energ.*, *34*(4), 1024–1032.
- Veneziano, D., and C. Lepore (2012), The scaling of temporal rainfall, *Water Resour. Res.*, *48*(8), W08516.
- Werner, E. E., C. J. Davis, D. K. Skelly, R. A. Relyea, M. F. Benard, and S. J. McCauley (2014), Cross-Scale Interactions and the Distribution-Abundance Relationship, *PLOS ONE*, *9*(5), e97387.

- Whitcher, B., and M. J. Jensen (2000), Wavelet estimation of a local long memory parameter, *Explor. Geophys.*, *31*(2), 94.
- Whitcher, B., P. Guttorp, and D. B. Percival (2000), Wavelet analysis of covariance with application to atmospheric time series, *J. Geophys. Res. Atmos.*, *105*(D11), 14941.
- Wu, J. (2006), *Scaling and Uncertainty Analysis in Ecology*, Methods and Applications, Springer Science & Business Media, Dordrecht, The Netherlands.
- Zhou, L., Y. Tian, R. B. Myneni, P. Ciais, S. Saatchi, Y. Y. Liu, S. Piao, H. Chen, E. F. Vermote, C. Song, and T. Hwang (2014), Widespread decline of Congo rainforest greenness in the past decade, *Nature*, *509*(7498), 86–90.
-

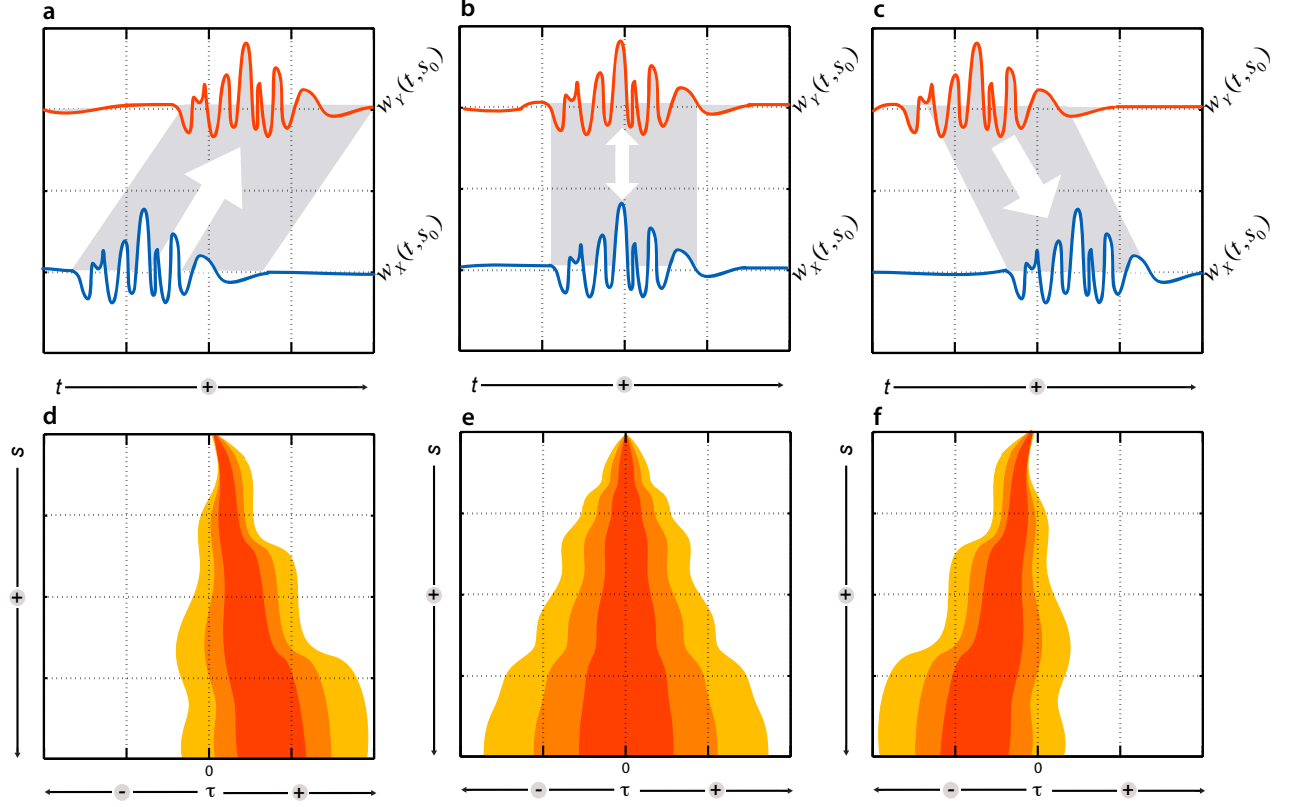


Figure 1. Conceptual representation of wavelet coefficients $w_i(t, s_0)$ for $i = X, Y$, as a function of time t and a fixed sample scale s_0 (a-c), and wavelet cross-correlation (d-f) for X driving Y (a,d), instantaneous coupling (b,e) and Y forcing X (c,f) for different scales s and time-lags τ (modified from *Molini et al.* [2010a]). The smallest temporal scale extracted in (d-f) is $s_1 = \frac{1}{2f_\nu}$, corresponding to the Nyquist frequency f_ν [see *Torrence and Compo*, 1998; *Mallat*, 2008; *Molini et al.*, 2010a, for further details]. Forcing direction is taken homogeneous across scales.

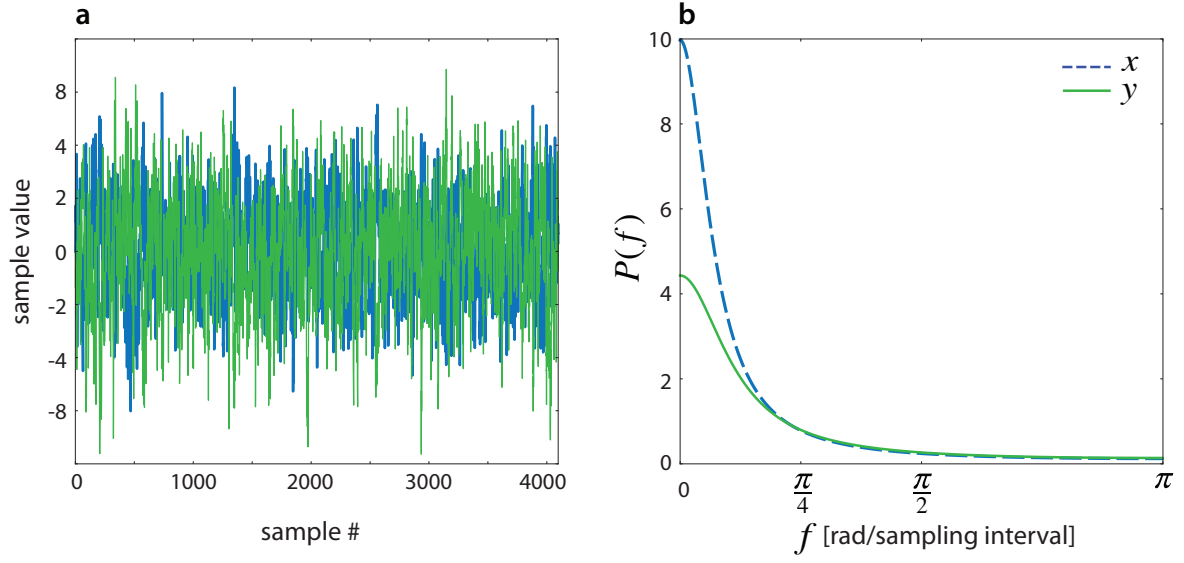


Figure 2. Sample realization of the VAR(1) system in equation (20) (a), and corresponding Lorentzian spectra $P(f)$ (b) for $C_1 = -0.4$ and $C_2 = 0$

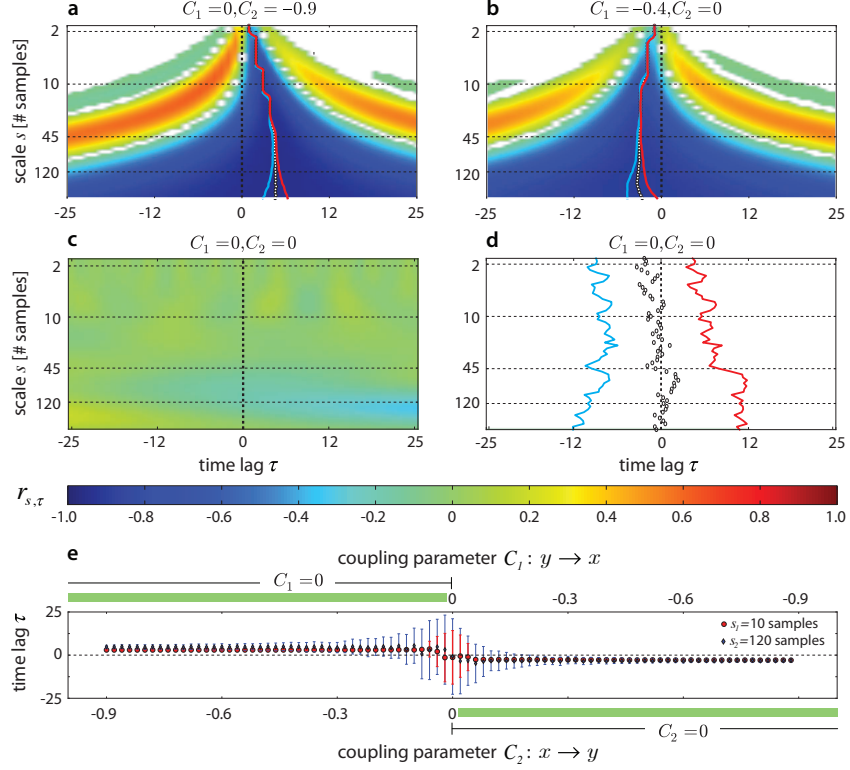


Figure 3. Ensemble and “single-realization” estimates of $r_{s,\tau}$ for the VAR(1) model in equation (20) and different coupling parameters C_1 and C_2 . Panels a and b respectively depict the ensemble estimates of $r_{s,\tau}$ for $x \rightarrow y$ ($C_1 = 0, C_2 = -0.9$) and $y \rightarrow x$ ($C_1 = -0.4, C_2 = 0$). Regions with $r_{s,\tau}$ below the $\alpha = 99\%$ significance level are masked in white. The same panels also show \bar{r}_{min} (black empty circles) as defined in section 3.1 and the corresponding 99% confidence intervals (blue and red solid lines) as a function of scale. Wavelet correlation patterns for the uncoupled system ($C_1 = C_2 = 0$) inferred from both a single realization, and an ensemble of simulations are shown in panels c and d, whereas panel e illustrates the sensitivity of \bar{r}_{min} to the coupling strength and directionality for sample scales $s_1 = 10$ (red dots) and $s_2 = 120$ (blue diamond) samples. Bottom and top x -axes in (e) respectively represent the coupling strength from from x to y (C_2) and y to x (C_1), whilst the red and blue bars are the confidence intervals of \bar{r}_{min} for $s = s_1$ and $s = s_2$ as in (a-b) and (d). Note how confidence intervals tend to widen with the weakening of the coupling, and moving from fine to large scales consistently with panels a-b and d.

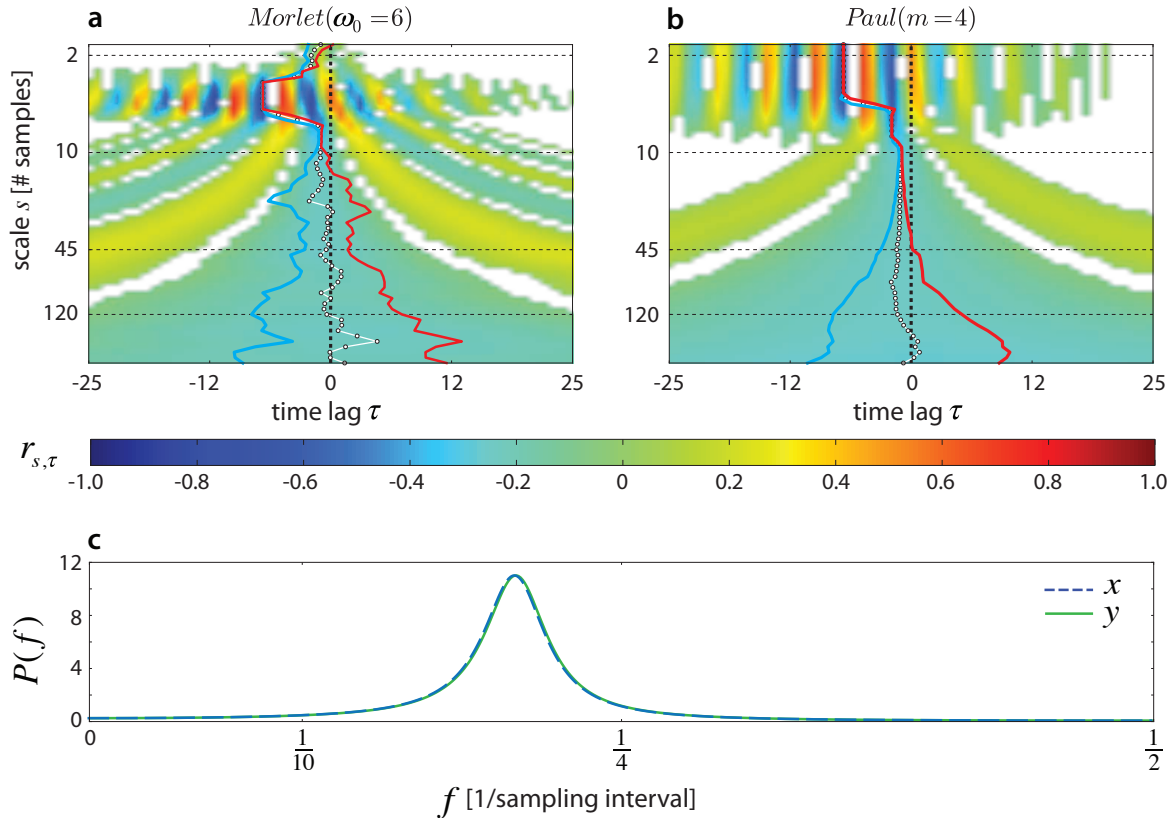


Figure 4. Ensemble estimates of $r_{s,\tau}$ and \bar{r}_{min} (same as in (a-b,d) of Figure 3) from the VAR(2) model in equation (21), obtained after pass-band filtering with the Morlet (a) and Paul (b) mother wavelets. Panel c shows the corresponding theoretical power spectra $P(f)$ of the auto-regressive sub-spaces of x and y . Here, both the Morlet and the Paul wavelets are able to capture the presence of the pronounced periodicity at $1/5$ of the cycle, in good agreement with the coupling peak shown in panel c for the theoretical spectra. However, Morlet’s wavelet, being more localized, can better resolve the coupling peak and its directionality, at the expense of a higher redundancy at large temporal scales.

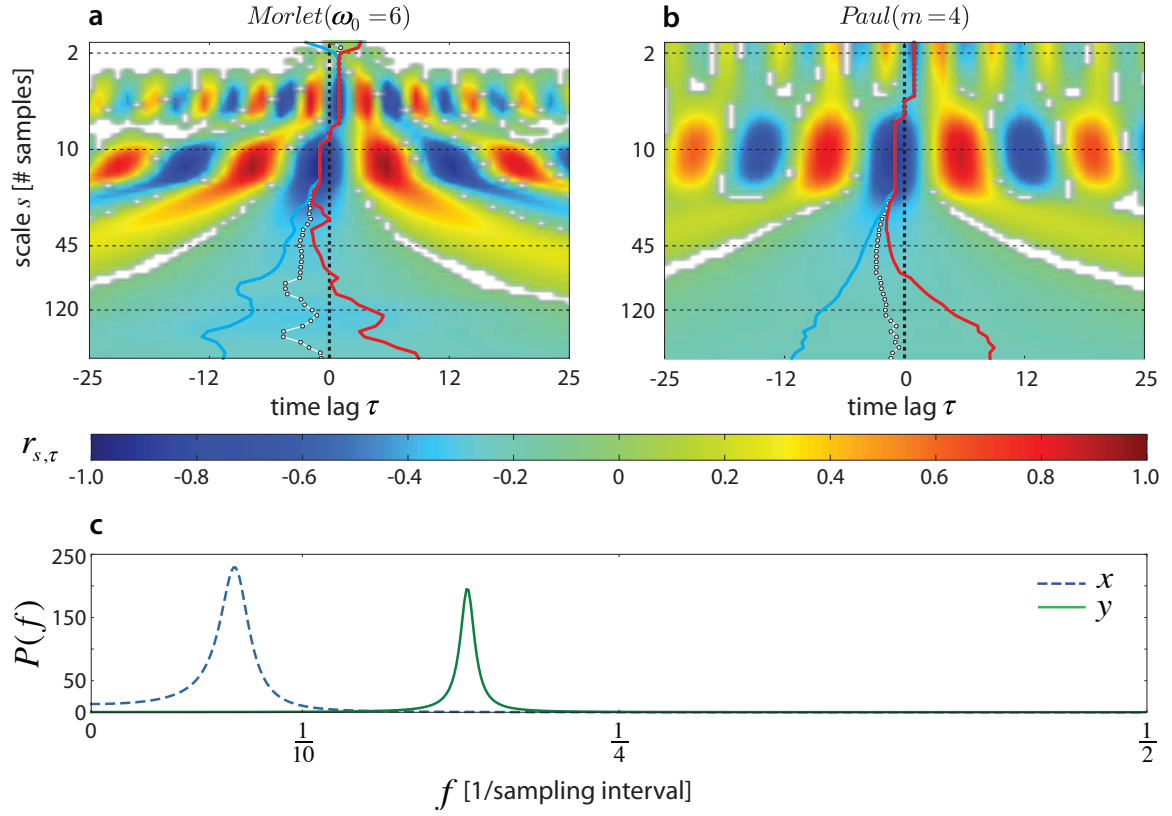


Figure 5. Same as Figure 4, but for a system with coupling and feedback occurring at $1/15$ of the cycle and $1/6$ of the cycle respectively, as described in equation (22).

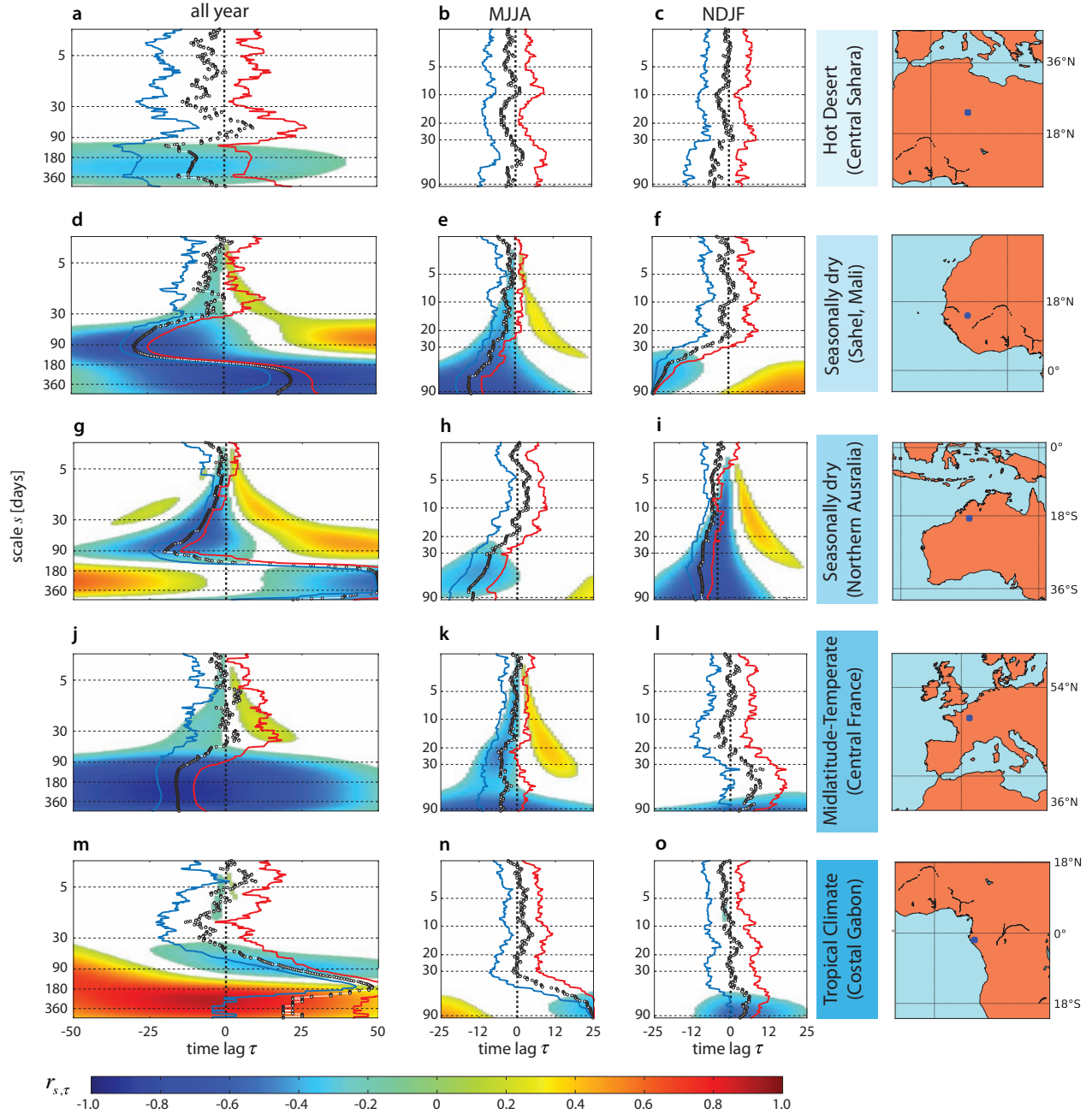


Figure 6. Ensemble estimates of $r_{s,\tau}$ and \bar{r}_{min} between soil moisture θ and air temperature T for five different geographical locations and climatic regimes. Right column shows the exact geographical location of the grid points used in the analysis. Left column reports the ensemble $r_{s,\tau}$ for the full time series at the specified location, while the central columns refers to Boreal summer (MJJA) and winter (NDJF) respectively. From top to bottom, panels are ordered by decreasing aridity.